A Comparative Study of Energy Management Schemes for a Fuel-Cell Hybrid Emergency Power System of More-Electric Aircraft

Souleman Njoya Motapon, *Member, IEEE*, Louis-A. Dessaint, *Fellow, IEEE*, and Kamal Al-Haddad, *Fellow, IEEE*

***Abstract*—This paper presents a comparative analysis of different energy management schemes for a fuel-cell-based emergency power system of a more-electric aircraft. The fuel-cell hybrid system considered in this paper consists of fuel cells, lithium-ion batteries, and supercapacitors, along with associated dc/dc and dc/ac converters. The energy management schemes addressed are state of the art and are most commonly used energy management techniques in fuel-cell vehicle applications, and they include the following: the state machine control strategy, the rule-based fuzzy logic strategy, the classical proportional–integral control strategy, the frequency decoupling/fuzzy logic control strategy, and the equivalent consumption minimization strategy. The main criteria for performance comparison are the hydrogen consumption, the state of charges of the batteries/supercapacitors, and the overall system efficiency. Moreover, the stresses on each energy source, which impact their life cycle, are measured using a new approach based on the wavelet transform of their instantaneous power. A simulation model and an experimental test bench are developed to validate all analysis and performances.**

***Index Terms*—Batteries, dc–dc converters, energy management, fuel cells, hybridization, optimization, supercapacitors.**

I. Introduction

OVER the last decade, the interest of transportation industries to develop efficient and environmentally friendly traction systems have made fuel-cell vehicles a reality. Nowadays, fuel cells are being used in cars, buses, tramways, trains, and aircraft [1]. They provide electrical power with high efficiency, less noise, and near zero emissions compared with conventional internal combustion engines.

As the first phase to greener aircraft, more-electric aircraft (MEA) manufacturers are moving toward replacing the emergency power system, which consists of a ram air turbine or an air-driven generator, by fuel-cell systems [4]–[6]. This will result in better performance of the emergency power system, particularly at low aircraft speed and altitude.

Manuscript received November 19, 2012; revised January 25, 2013; accepted March 3, 2013. Date of publication April 5, 2013; date of current version August 23, 2013. This work was supported in part by the Natural Sciences and Engineering Research Council of Canada, in part by the Consortium for Research and Innovation in Aerospace in Québec, and in part by Bombardier Aerospace and Transtronic Inc. under the CRIAQ ENV405 Project.

The authors are with the Power Electronics and Industrial Control Research Group (GREPCI), Ecole de Technologie Superieure, Montreal, QC H3C 1K3, Canada (e-mail: souleman_motapon@yahoo.fr; dessaint@ele.etsmtl.ca; kamal.al-haddad@etsmtl.ca).

Color versions of one or more of the figures in this paper are available online at http://ieeexplore.ieee.org.

Digital Object Identifier 10.1109/TIE.2013.2257152

To improve the dynamics and power density of fuel-cell systems, hybridization of fuel cells with new energy storage devices such as lithium-ion batteries or supercapacitors is required. This hybridization allows the fuel-cell system to be optimized to achieve better fuel economy and performance as part of the load is provided by the batteries/supercapacitors. This optimization is accomplished through an energy management strategy (EMS), which distributes the load power among the energy sources. The design of such an EMS should be made in such a way to achieve an optimal fuel economy while ensuring that each energy source operates within its limits. In addition, the EMS impact on the life cycle of the whole hybrid power system should be limited as possible.

Different energy management strategies for fuel-cell hybrid power systems have been reported in the literature. The use of state machine control [8], [9] is a simple and well-known rule-based strategy; each EMS rule or state is defined based on heuristic or empiric past experience. Therefore, the performance of this strategy depends on how well the designer is familiar with the operation of each component in the system.

Another widely used strategy is the rule-based fuzzy logic energy management technique, where the power distribution is accomplished through membership functions and the set of IF–THEN rules [10], [11]. This strategy can be easily tuned to achieve optimal operation, and its performance is less sensitive to measurement imprecision and component variations. Nevertheless, the heart of the fuzzy logic controller resides on the IF–THEN rules, which require the knowledge and past experience of an expert.

Recently, energy management based on classical PI controllers have been proposed. This strategy is based on the control of the main performance parameters, such as the battery state of charge (SOC), the supercapacitor voltage, or dc-bus voltage using proportional–integral (PI) controllers [1]–[3]. The knowledge of an expert is not necessary, and the PI controllers can be easily tuned online for better tracking. The load power is distributed in such a way to allow the fuel-cell system to provide the steady-state load demand.

The frequency decoupling strategy ensures that the fuel cell provide low frequency demand, whereas the other energy sources deal with high frequency demand [12], [13]. This is achieved through the use of low-pass filter, wavelet, or fast Fourier transform techniques. This strategy improves the lifetime of the fuel-cell system as the dynamic stress on the fuel supply system is prevented. Here, the fuel-cell system supplies

a nearly constant mean load power, whereas the other energy sources discharge or recharge when the load power is above or below its mean value, respectively.

To ensure optimal operation of the fuel-cell system for maximum fuel economy or maximum global efficiency, a cost function optimization strategy is used [14], [15]. The most common strategy for real-time implementation is the equivalent fuel consumption minimization strategy (ECMS). The power distribution is determined from the minimization of an instantaneous cost function, which consists of the fuel consumption of the fuel-cell system and the equivalent fuel consumption of the other energy sources.

Other real-time energy management strategies for fuel-cell hybrid power systems have also been reported. They include strategies based on model predictive control [18], stochastic dynamic programming [19], neural networks [20], adaptive optimal control [21], and H-infinity control [22]. These strategies are very complex and require large computations, which could potentially affect the response time of the energy management system. This paper deals only with the most common and easily realizable energy management strategies using standard microprocessor-based solutions.

Most of the comparative studies of EMS found in the literature are mainly applied to a hybrid vehicle load profile, which is regenerative with low fluctuations compared with an aircraft emergency load profile. Moreover, these studies include only a few of the existing EMSs, and their impact on the overall efficiency and life cycle of the whole system are often omitted [22], [23]. This has motivated the authors of this paper for further analysis to determine which EMS fits better with the MEA load profile.

The main goals of this paper are to design and compare different energy management techniques for a fuel-cell hybrid emergency power system of MEA. The main criteria for performance comparison are the hydrogen consumption, the SOCs of batteries and supercapacitors, the overall system efficiency, and the stresses seen by each energy sources.

The energy management strategies implemented for comparison are the following:

- state machine control strategy [8];
- rule-based fuzzy logic strategy [10], [11];
- classical PI control strategy [1], [2];
- frequency decoupling and fuzzy logic strategy [12], [13];
- ECMS [14]–[16].

Using a typical emergency mission profile of a MEA, the energy management strategies are compared through simulation and experimentally using a 14-kW fuel-cell hybrid power system test bench. The models developed require standard parameters, which can be found on manufacturer datasheet or through simple experiments for better accuracy.

The main contribution of this paper is a validated performance comparison of common EMS strategies for an aircraft emergency system based on fuel cells. The analysis includes the EMS impact on the overall efficiency and life cycle of the whole system. The latter is measured using a new approach based on the wavelet transform of each energy source instantaneous power.

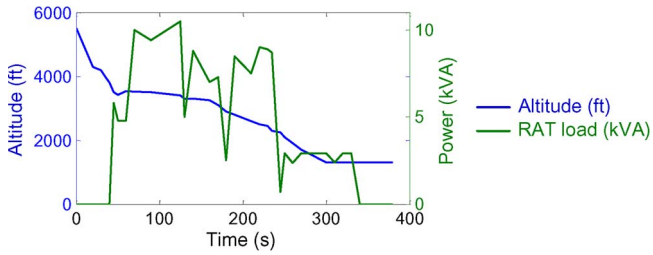

Fig. 1. Load profile of a typical emergency landing cycle.

The paper is organized as follows. Section II describes the hybrid power system architecture. Section III deals with components modeling and validation. Section IV presents the energy management strategies. Section V compares the strategies through simulation and experimentation. Finally, this paper ends with a conclusion.

II. Hybrid Emergency Power System Architecture

The hybrid power system is designed based on the power and energy requirement for a typical emergency landing scenario. In this paper, a representative emergency landing cycle (see Fig. 1), provided by Bombardier Aerospace, is considered for all analysis.

The fuel-cell system is designed to meet the average demand (7.5 kW), whereas the batteries and supercapacitors are designed to assist the latter during continuous and transient peak demand, respectively. For simplicity, detail analysis on the design and topology selection is not covered in this paper. However, for references, the hybrid system is designed following the procedure in [1], and the topology adopted is discussed in [7]–[9].

Fig. 2 shows the system schematic where four of the Valence battery modules (12.8 V, 40 Ah) are used along with six NESSCAP supercapacitor modules (48.6 V, 88 F). The fuel-cell system consists of a 12.5-kW proton exchange membrane (PEM) fuel-cell power module (FCPM) from Hydrogenics.

As shown in Fig. 2, the fuel-cell energy and battery energy are controlled through their associated dc/dc converters using a National Instrument embedded controller (NI PXI-8108). The dc/dc converters require an output voltage reference and a maximum input/output current reference, which are determined from the energy management system (implemented in the controller). For this paper, two converters are used with the battery system due to time constraint as the bidirectional dc/dc converter was not readily available. A battery management system (BMS) is used to protect the battery system from overcharge, overtemperature, and overdischarge. A protecting resistor is also used to prevent the overvoltage of supercapacitors or the inverter input voltage. The emergency load profile is generated using an ac/dc programmable load.

For this paper, off-the-shelf components are selected as the primary goal is to investigate the performance of different energy management strategies. In other words, the power density factor, which is crucial for the integration of the system on an aircraft, is not considered at this point.

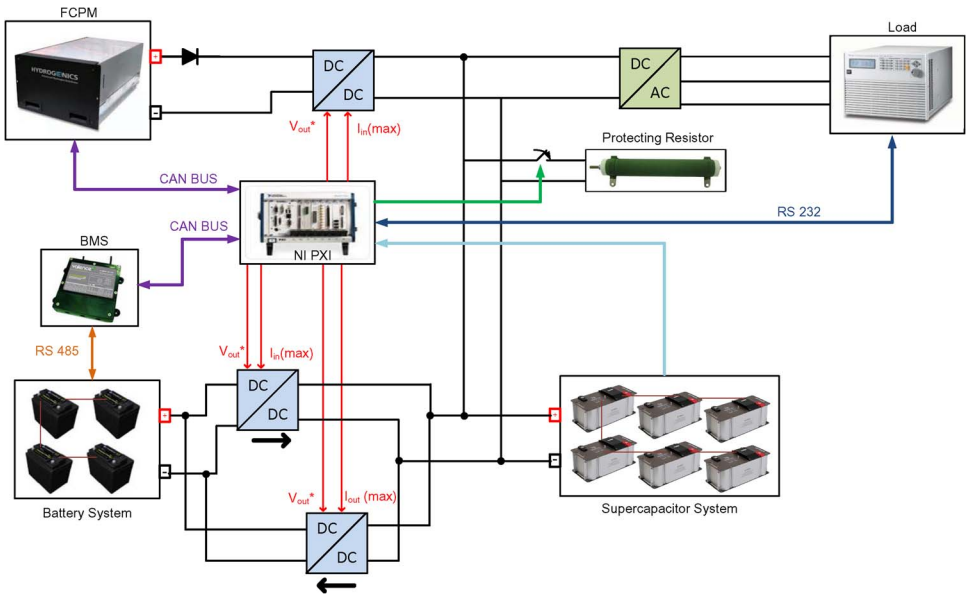

Fig. 2. Overall system schematic.

The main characteristics of the hybrid power system are as follows.

- The fuel-cell system: It is a 12.5-kW 60–30-V_{dc} liquid-cooled PEM FCPM with built-in auxiliaries (air blower, filter, H_2 recirculation pump, H_2 pressure regulator and valves, coolant pump and fans, etc.). The FCPM is also equipped with a built-in controller (engine control unit) for interfacing with the main controller and protections (H_2 low pressure, stack over temperature, over current, and under voltage).
- The battery system: It consists of four 12.8-V 40-Ah Li-ion battery modules connected in series. Each module is equipped with an internal controller for cell-to-cell balancing (or intramodule balancing), cell temperature and voltage/current sensing, SOC calculation, and communication with an overall BMS through RS485.
- The supercapacitor system: It consists of six 48.6-V 88-F supercapacitor modules connected in series. Each module is also equipped with an internal controller (ultracapacitor management unit) for cell-to-cell balancing and voltage and temperature sensing.
- The fuel-cell dc/dc converter system: It consists of five (40–64 V) dc-in 270-V (adjustable 243–297 V) 9.2-$A_{dc\ out}$ dc/dc isolated boost converters connected in parallel. The system is equipped with overload and overvoltage protection for each module. Redundant operation is possible with the use of decoupling diodes. Current balancing is achieved by active current sharing. The output voltage and the input current are adjusted by external signals (0–10 V).
- The battery dc/dc converter system: It consists of two (40–58.4 V) dc-in 270-V (adjustable 243–297 V) 7-$A_{dc\ out}$ dc/dc isolated boost converters connected in parallel, together with a single (243–297 V) dc-in 48-V (adjustable 0–58.4 V) 20-$A_{dc\ out}$ (max) dc/dc isolated buck converter. All converters feature similar characteristics as the fuel-cell dc/dc converter.
- The inverter system: It consists of three (160–320 V) dc-in 200-V_{ac} 400-Hz 5-kVA dc/ac isolated converters connected in parallel. The system is equipped with overload, overvoltage, and short-circuit protection. Each converter output voltage is regulated to the nominal voltage with a total harmonic distortion of less than 3%.
- The programmable dc/ac load: It consists of six 4.5-kW 45-A 350-V electronically programmable loads. Each load is equipped with a digital signal processor to emulate nonlinear/linear ac (45–440 Hz) or dc load.
- Sensors and signals conditioning: There are voltage and current sensors at each converter input/output. Each device temperature is obtained from the built-in controller or thermistors. Signal conditioning is achieved through NI data acquisition cards.

The following deals with the modeling of all these components and describes them in more details.

III. Modeling of the Hybrid Emergency Power System

In the study of energy management strategies, it is necessary to develop a full and quite accurate model of each subsystem components. This helps in understanding the system behavior and allows an effective design of the energy management system. This section describes the modeling approach of each component of the hybrid power system.

A. Fuel-Cell Model

PEM fuel cells are the most common fuel cells used for automotive application. This is mainly due to the fact that they operate at low temperature $(-20\ ^{\circ}\mathrm{C}-100\ ^{\circ}\mathrm{C})$; therefore, fast starting from idle to full load operation can be achieved.

The model of the hybrid system is made in MATLAB/Simulink using the SimPowerSystems (SPS) toolbox, which contains a fuel-cell stack model. The SPS fuel-cell model is

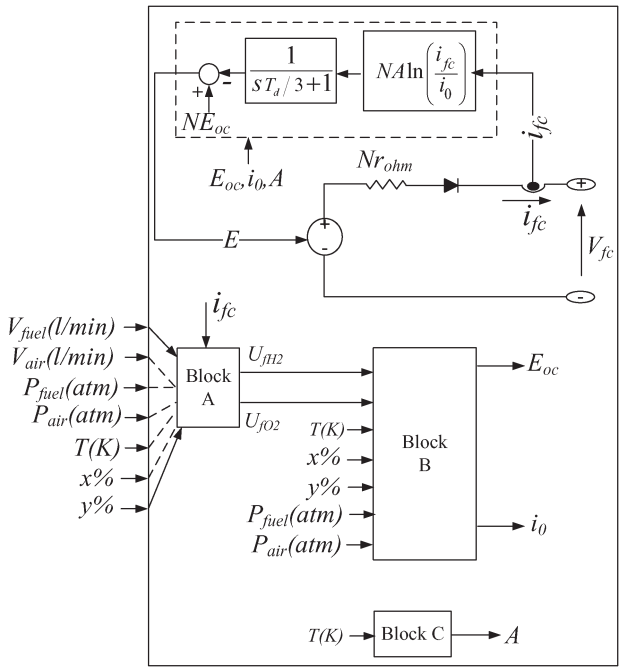

Fig. 3. Fuel-cell stack model.

a modified version of the approach proposed in [24], where the dynamics of the reactant flow inside the electrode are neglected. Hence, the determination of partial pressure of reactants is decoupled from the electrode characteristics (such as anode/cathode volume and orifice area). An interesting feature of this model is the fact that the model parameters can be obtained from datasheet or from a simple polarization curve test.

This model is selected for this paper and the main equations are as follows [25].

The cell output voltage, considering the losses due to reaction kinetics (activation losses) and charge transport (resistive and diffusion losses) is given by

$$V = E_{\rm oc} - V_{\rm act} - V_r \tag{1}$$

with

$$V_{\rm act} = A \ln\left(\frac{i_{\rm fc}}{i_0}\right) \cdot \frac{1}{sT_d/3+1} \tag{2}$$

$$V_r = r_{\rm ohm} \cdot i_{\rm fc} \tag{3}$$

where A is the Tafel slope (in volts), i_0 is the exchange current (in amperes), $r_{\rm ohm}$ is the combined cell and diffusion resistance (in ohms), T_d is the cell settling time to a current step. It is assumed that the cell voltage will exhibit a delay approximately equal to three times the time constant during a sudden change in cell current.

The fuel-cell stack (multiple cells in series) output voltage is derived by knowing the number of cells as

$$V_{\rm fc} = N \cdot V \tag{4}$$

where N is the number of cells.

Fig. 3 shows the model of the fuel-cell stack implemented in SPS. The parameters required by the model are obtained from a polarization curve test on the FCPM. This test is shown in Fig. 4, where the FCPM electrical output is directly connected to the programmable load. As soon as the FCPM is started at no load, current steps are applied following the fuel-cell maximum allowable current. This allows observing both the steady and transient performances of the FCPM with the load demand, necessary for validation purposes. The parameters required by the model are shown in Fig. 5, along with the simulated polarization curves.

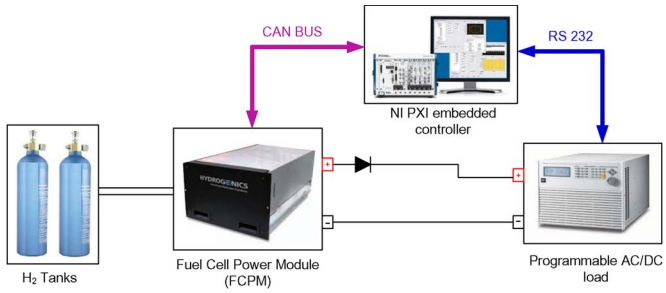

Fig. 4. Fuel-cell experimental setup.

Fig. 6 shows the simulation and test results (at nominal condition, $P_{\rm fuel} = 1.16$ bar, $P_{\rm air} = 1$ bar, and $T = 45$ °C) along with the percentage error between the simulated and the real fuel-cell output voltage.

It can be observed in Fig. 6 that, in the activation region (region with predominant activation losses), the steady-state error is within $\pm 1\%$, whereas the transient errors are within $\pm 4\%$. In the ohmic region (region with predominant resistive losses), the error is also within $\pm 1\%$ for both transient- and steady-state conditions. This low error indicates that the fuel-cell system behavior is well represented by the model. More details on the validation of the SPS fuel-cell model can be found in [25].

B. Battery Model

The batteries considered for this paper are of type Li-ion as they have proven to exhibit high energy density and efficiency compared with other battery types (such as lead-acid, NiCd or NiMH) [16], [17]. This makes them more attractive for automotive or aircraft applications.

The battery model available in SPS is used for this paper. This model is based on a modified Shepherd curve-fitting model, where an additional term (voltage polarization) is added to the battery discharge voltage expression to better represent the effect of the battery SOC on the battery performance. In addition, to ensure the simulation stability, a filtered battery current, instead of the actual battery current, is used to account for the polarization resistance. Similar to the fuel-cell model, the model parameters are easily derived from datasheets or simple dynamic tests.

The main equations for a Li-ion battery type are given as follows [26].

The battery voltage is expressed as

$$V_{\rm batt} = E_0 - K\frac{Q}{Q-it} \cdot it - R_b \cdot I + A_b \exp(-B \cdot it) - K\frac{Q}{Q-it} \cdot i^* \tag{5}$$

FUEL CELL MODEL INPUT PARAMETERS	
Voltage @ 0 A and 1 A [V_0 (V), V_1 (V)]	[52.5, 52.46]
Nominal operating point [Inom (A), Vnom (V)]	[250, 41.15]
Maximum operating point [Iend (A), Vend (V)]	[320, 39.2]
Number of cells	65
Nominal stack efficiency (%)	50
Operating temperature (Celcius)	45
Nominal Air flow rate (lpm)	732
Nominal supply pressure [Fuel (bar), Air (bar)]	[1.16, 1]
Nominal composition (%) [H2, O2, H2O (Air)]	[99.95, 21, 1]
Fuel cell voltage response time (sec)	1
Peak O2 utilization (%)	60
Voltage undershoot (V) @ Peak O2 utilization	2

(a)

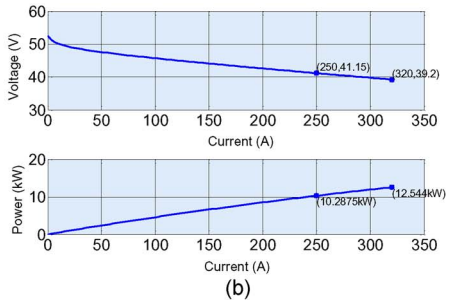

(b)

Fig. 5. Fuel-cell stack model. (a) Input parameters. (b) Polarization curves.

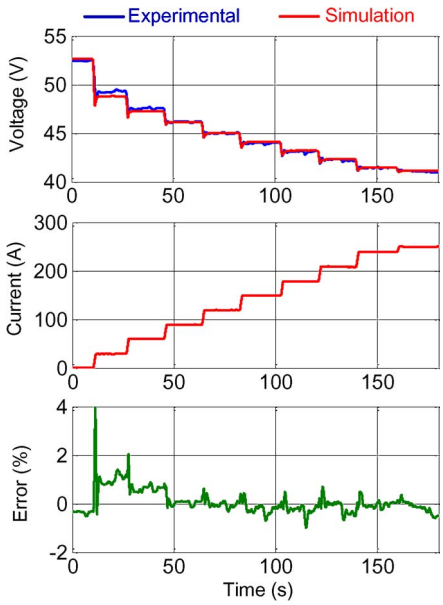

Fig. 6. Fuel-cell model validation. Simulation versus experimental results of the 12.5-kW FCPM. $P_{\text{fuel}} = 1.16$ bar. $P_{\text{air}} = 1$ bar. $T = 45\ ^{\circ}\text{C}$.

where E_0 is the battery constant voltage (in volts), K is the polarization constant (in volts per ampere-hour), Q is the battery capacity (ampere-hour), i^* is the filtered battery current (in amperes), it is the actual battery charge (in ampere-hours), A_b is the exponential zone amplitude (in volts), B is the exponential zone time constant inverse (in Ah^{-1}), and R_b is the battery internal resistance (in ohms).

The term $K(Q/(Q-it))it$ from (5) is referred as polarization voltage, whereas the term $K(Q/(Q-it))$ is the polarization resistance Pol_{res}.

During charging, the battery voltage increases abruptly after being fully charged; this behavior is represented by modifying the polarization resistance (only during charging) as follows:

$$\text{Pol}_{\text{res}} = K\frac{Q}{it - 0.1Q}. \tag{6}$$

Fig. 7 shows the model of the battery implemented in SPS. The experimental setup used to obtain the battery model parameters and for validation purpose is shown in Fig. 8. As shown, the superpacitors are used to discharge and recharge the batteries. The charge and discharge currents are controlled through dc/dc converters. This setup allows observing the steady and transient performances of the battery/supercapacitor modules with the load demand, during charging and discharging modes.

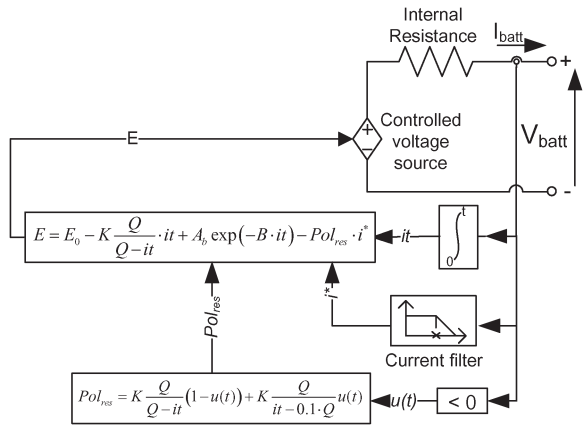

Fig. 7. Li-ion battery model.

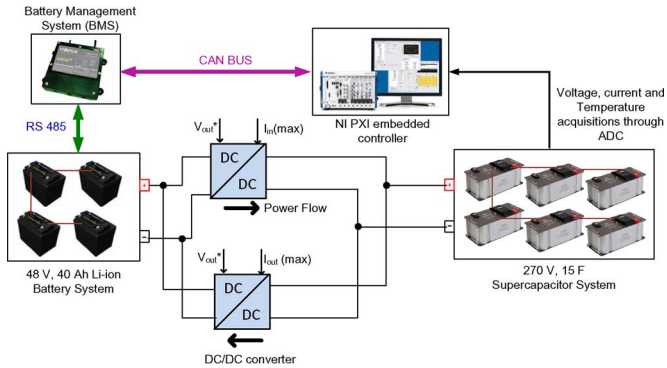

Fig. 8. Experimental setup of battery and supercapacitor systems.

Fig. 9 shows the model input parameters along with simulated discharge curves for the battery system (four 12.8-V 40-Ah valence Li-ion battery modules).

Fig. 10 shows the simulation and test results along with the percentage error between the simulated and the real battery system output voltage. The obtained error is less than $\pm 2\%$ for both transient- and steady-state conditions, which confirms the validity of the battery model. More details on the validation of the SPS battery model can be found in [26].

C. Supercapacitor Model

Supercapacitors, which are also known as electric double-layer capacitors (EDLCs) are similar to conventional

BATTERY MODEL INPUT PARAMETERS	
Nominal Voltage (V)	48
Rated Capacity (Ah)	40
Maximum Capacity (Ah)	40
Fully Charged Voltage (V)	55.88
Nominal Discharge Current (A)	17.4
Internal Resistance (ohms)	0.012
Capacity (Ah) @ Nominal Voltage	36.17
Exponential Zone [Voltage (V), Capacity (Ah)]	[52.3, 1.96]
Battery Voltage response time (sec)	30

(a)

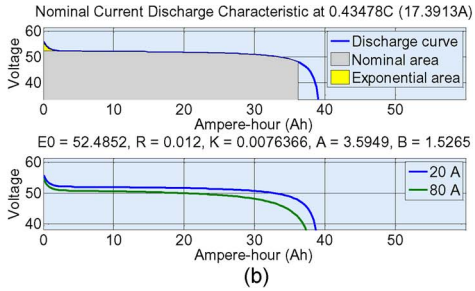

(b)

Fig. 9. Battery model. (a) Input parameters. (b) Discharge curves.

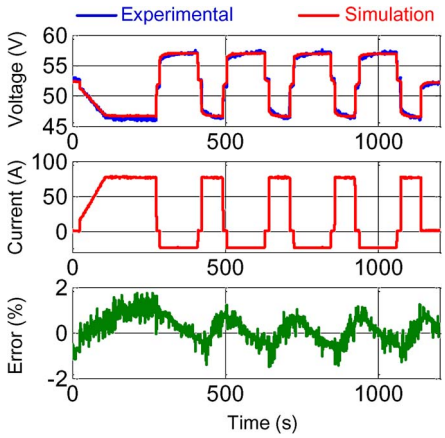

Fig. 10. Battery model validation. Simulation versus experimental results. Charge and discharge of the 48-V 40-Ah Li-ion battery system.

electrostatic or electrolytic capacitors, with the advantage that they can store or release more energy due to their high capacitance [27].

The supercapacitor model implemented in SPS is based on the Stern model, which combines the Helmholtz and Gouy–Chapman models [28]. The capacitance of an EDLC cell is expressed as

$$C = \left[\frac{1}{C_H} + \frac{1}{C_{\rm GC}}\right]^{-1} \tag{7}$$

with

$$C_H = \frac{N_e \varepsilon \varepsilon_0 A_i}{d} \tag{8}$$

$$C_{\rm GC} = \frac{FQ_c}{2N_e RT} \sinh\left(\frac{Q_c}{N_e^2 A_i \sqrt{8RT\varepsilon\varepsilon_0 c}}\right) \tag{9}$$

where C_H and $C_{\rm GC}$ are the Helmholtz and Gouy–Chapman capacitance (in farads), respectively; N_e is the number of electrode layers; and ϵ and ϵ_0 are the permittivity values (in farads per meter) of the electrolyte material and free space, respectively. A_i is the interfacial area between electrodes and electrolyte (in square meters), d is the Helmholtz layer length (or molecular radius) (in meters), Q_c is the cell electric charge (in coulomb) and c is the molar concentration $(\text{in mol} \cdot \text{m}^{-3})$.

For a supercapacitor module of N_s cells in series and N_p cells in parallel, the total capacitance is given by

$$C_T = \frac{N_p}{N_s} \cdot C. \tag{10}$$

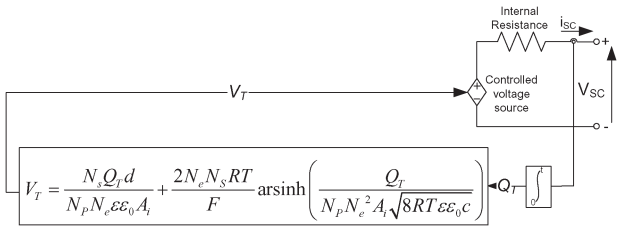

Fig. 11. Supercapacitor model.

The supercapacitor output voltage is expressed considering resistive losses as

$$V_{\rm SC} = \frac{Q_T}{C_T} - R_{\rm SC} \cdot i_{\rm SC} \tag{11}$$

with

$$Q_T = N_p Q_c = \int i_{\rm SC} dt \tag{12}$$

where Q_T is the total electric charge (in coulombs), $R_{\rm SC}$ is the supercapacitor module resistance (in ohms), and $i_{\rm SC}$ is the supercapacitor module current (in amperes).

Fig. 11 shows the model of the supercapacitor implemented in SPS. The critical parameters required by the model are obtained from the specifications (rated capacitance and voltage, and dc resistance), whereas the number of electrode layers and the molecular radius are adjusted for better accuracy based on experiments. Fig. 12 shows the model input parameters along with simulated discharge curves for the supercapacitor system.

The simulation and test results are shown in Fig. 13, along with the percentage error between the simulated and the real supercapacitor system output voltage. It can be observed that the accuracy of the model is within $\pm 2\%$, which is sufficient for this paper.

D. DC/DC Converter Model

The fuel-cell and battery systems are connected to the dc/ac converter through dc/dc converters. This allows voltage conversion (from low voltage to high voltage and *vice versa*) as well as full control of the fuel-cell/battery current and dc-bus voltage. The fuel-cell system dc/dc converter is of boost type, whereas the battery system converters consist of one dc/dc converter of boost type (discharge converter) and one dc/dc converter of buck type (charge converter).

DC/DC converters can be represented by two types of models, which are the switching models and the average-value

SUPERCAPACITOR MODEL INPUT PARAMETERS	
Rated Capacitance (F)	15.6
Equivalent Series Resistance DC (Ohms)	0.15
Rated Voltage (V)	291.6
Surge Voltage (V)	307
Number of Series Capacitor	108
Number of Parallel Capacitor	1
Number of Layer*	6
Molecular Radius (m)*	0.4×10^{-9}
Operating Temperature (°C)	25

*Estimated

(a)

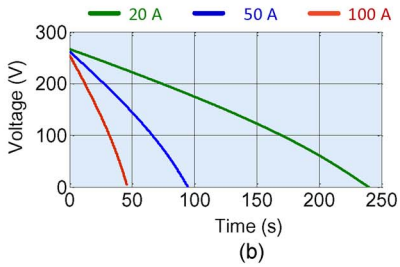

(b)

Fig. 12. Supercapacitor model. (a) Input parameters. (b) Discharge curves.

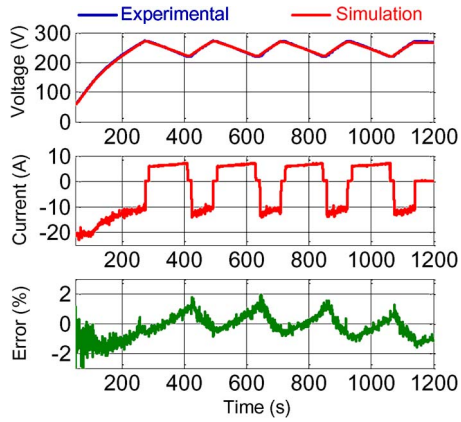

Fig. 13. Supercapacitor model validation. Simulation versus experimental results. Charge and discharge of the 270-V 15-F supercapacitor system.

model. The switching models are mainly used for design purposes and to investigate types of pulsewidth-modulated schemes with regard to switching harmonics and losses. These models require low sampling time to observe all the switching actions, which makes the simulation very time consuming. The average-value models on the contrary are less time-consuming as the switches are replaced by controlled voltage/current sources. The switching harmonics are not represented, but all the converter dynamics are maintained, which makes these models attractive as larger sampling time can be used.

Average value dc/dc converter models are used in this paper, as shown in Fig. 14. The design of the control loops is made considering the model dynamics.

The model performances are shown in Fig. 15. As shown, the converter models and the real converters have very close responses to load changes, as well as during overload. The voltage is well regulated, and the current is well limited to its maximum reference current. For the fuel-cell system, the slow response obtained both experimentally and in simulation is due to the current slope limitation (40 A/s) to deal with the problem of oxygen starvation.

E. DC/AC Converter Model

Similar to the dc/dc converter model, the dc/ac converter is represented by an average-value model shown in Fig. 16. A three-phase 200-V 400-Hz voltage signal is the reference for the voltage-controlled sources. The input current is obtained from the generated output power and dc-bus voltage.

The performance of the dc/ac converter model is shown in Fig. 17. As observed, the model behaves as the real converter with similar response during a load step.

F. Emergency Load Model

The load is represented by a three-phase controlled current source, where the load current is obtained from the three-phase apparent power (in kilovoltamperes) load profile, the power factor, and the nominal line voltage.

IV. Energy Management Strategies

The energy management system is required to ensure the following:

- low hydrogen consumption;
- high overall system efficiency;
- narrow scope of the battery/supercapacitor SOC;
- long life cycle.

This is achieved by controlling the power response of each energy source with load demand through their associated converters, using a given EMS. For this paper, five state-of-the-art EMSs are considered and designed based on the requirements given in Table I.

The dc-bus voltage (or supercapacitor SOC) is regulated through the battery converters for all EMS strategies, as shown in Fig. 18(f). The main difference between the EMS relies on the approach to obtain the fuel-cell reference power. The following sections describe the EMS considered in detail.

A. State Machine Control Strategy

The state machine control strategy implemented consists of eight states, as shown in Table II. These states are derived using the same approach proposed in [8]. The fuel-cell power is determined based on the battery SOC range and load power P_{load}. The EMS scheme is depicted in Fig. 18(a). One drawback of this method is the fact that a hysteresis control (shown in Fig. 19) is required when switching the states, which affects the response of the EMS to changes in load demand.

B. Rule-Based Fuzzy Logic Strategy

This scheme has a faster response to load change compared with state machine control and is more robust to measurement imprecision. The fuel-cell power is obtained based on the

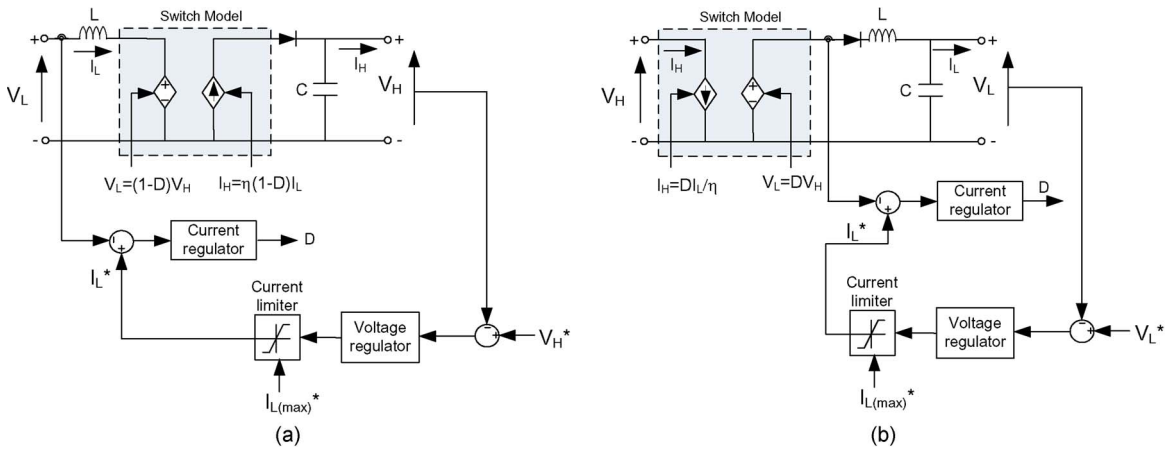

Fig. 14. dc/dc converter model. (a) Boost type. (b) Buck type.

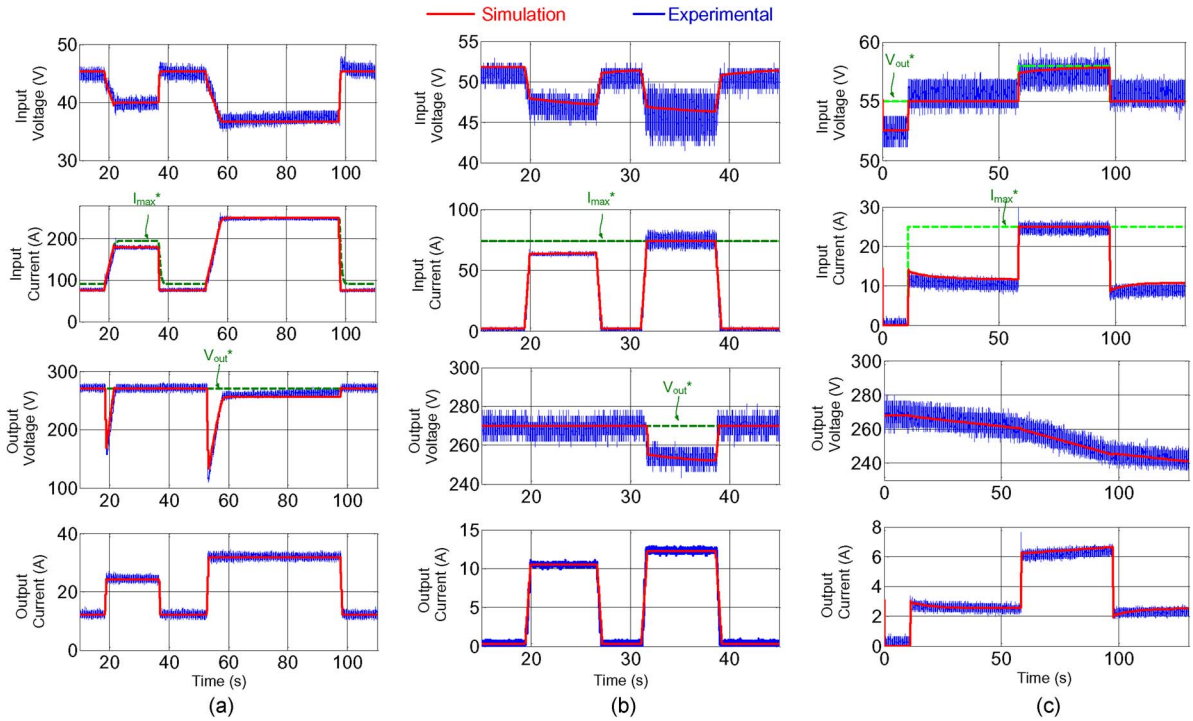

Fig. 15. DC/DC converter model validation. (a) Fuel-cell boost converter. (b) Battery boost converter. (c) Battery buck converter.

load power and SOC membership functions and the set of IF–THEN rules. The scheme is shown in Fig. 18(b). The design is made following an approach similar to [10] where trapezoidal membership functions are used, as shown in Fig. 20. The fuzzy logic rules are derived from the state machine control decisions, as shown in Table III. The Mamdani's fuzzy inference approach is used along with the centroid method for defuzzification.

C. Classical PI Control Strategy

This scheme controls the battery SOC using a PI regulator [1], as shown in Fig. 18(c). The output of the PI regulator is the battery power, which is afterward removed from the load power to obtain the fuel-cell reference power. When the battery SOC is above the reference, the fuel-cell power is low, and the battery provides its full power. When the SOC is below the reference, the fuel cell provides almost the load power. This scheme is easier to implement compared with previous strategies, and the PI gains are tuned online for a better response.

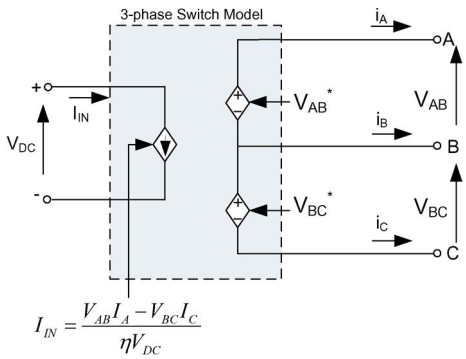

Fig. 16. DC/AC converter model.

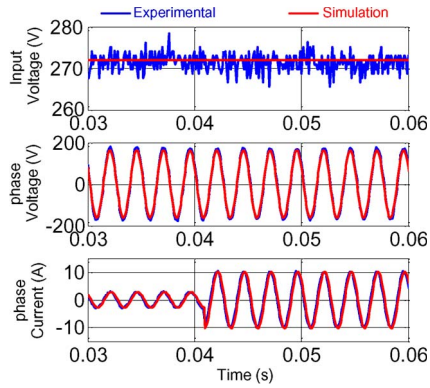

Fig. 17. DC/AC converter model validation.

TABLE I
ENERGY MANAGEMENT DESIGN REQUIREMENTS

ENERGY MANAGEMENT DESIGN REQUIREMENTS	
Fuel cell power [Pfc_{min} - Pfc_{max}] (kW)	[1 - 10]
Battery power [$Pbatt_{min}$ - $Pbatt_{max}$] (kW)	[-1.2 - 4]
Battery state of charge [SOC_{min} - SOC_{max}] (%)	[60 - 90]
DC bus voltage [Vdc_{min} - Vdc_{max}] (V)	[250 - 280]
Fuel cell current maximum slope (A/s)	40

D. Frequency Decoupling and Fuzzy Logic Strategy

The frequency decoupling and fuzzy logic strategy allows the fuel-cell system to provide a low frequency load demand, whereas the other energy sources deal with the high frequency demands [13]. The main advantage with this method is the fact that the mean energy of the battery is close to zero, which ensures a narrow scope of the battery SOC. Nevertheless, a fuzzy logic controller is required to control the battery SOC around a minimum limit. The scheme is shown in Fig. 18(d), where a low-pass filter is used for frequency decoupling. The cutoff frequency of the filter is set to 8 mHz, which allows the fuel cell to provide a nearly constant power. The fuzzy logic controller is the same as in the rule-based fuzzy logic strategy.

E. ECMS

The ECMS is a well-known instantaneous cost-function-based optimization strategy used by several authors [14]–[16]. The goal is to achieve a minimum fuel consumption by minimizing the fuel consumed by the fuel cell and the equivalent fuel required to maintain the battery SOC. The approach proposed in [16] is used in this paper where the battery SOC is controlled through the penalty coefficient of the battery energy. The scheme is shown in Fig. 18(e). The optimization problem is defined as follows.

Find an optimal solution $x = [P_{\rm fc}, \alpha, P_{\rm batt}]$, which minimizes

$$F = [P_{\rm fc} + \alpha P_{\rm batt}] \cdot \Delta T \tag{13}$$

under the equality constraints

$$P_{\rm load} = P_{\rm fc} + P_{\rm batt} \tag{14}$$

$$\alpha = 1 - 2\mu \frac{(\mathrm{SOC} - 0.5(\mathrm{SOC}_{\max} + \mathrm{SOC}_{\min}))}{\mathrm{SOC}_{\max} + \mathrm{SOC}_{\min}} \tag{15}$$

within the boundary conditions

$$P_{\rm fc\,min} \le P_{\rm fc} \le P_{\rm fc\,max}$$

$$P_{\rm batt\,min} \le P_{\rm batt} \le P_{\rm batt\,max}$$

$$0 \le \alpha \le 100$$

where $P_{\rm fc}$, $P_{\rm batt}$, and $P_{\rm load}$ are the fuel-cell power, battery power, and load power, respectively (considering the converter losses). α is the penalty coefficient, and μ is a constant (adjusted to 0.6 for better control of the battery SOC). ΔT is the sampling time. $P_{\rm fc\,min}$ and $P_{\rm fc\,max}$ are the minimum and maximum fuel-cell power, respectively. $P_{\rm batt\,min}$ and $P_{\rm batt\,max}$ are the minimum and maximum battery power, respectively. $\mathrm{SOC}_{\min}$ and $\mathrm{SOC}_{\max}$ are the minimum and maximum battery SOCs, respectively.

The supercapacitor power is not considered in the optimization problem as the dc-bus voltage is controlled by the battery converters. That is, as soon as the supercapacitors discharge, they are recharged with the same energy from the battery system. Therefore, the total load energy is shared only between the fuel cell and the battery over a given load cycle.

V. Simulation and Experimental Results

The performances of the EMS were compared using simulations and experimental tests on the 14-kW fuel-cell hybrid system (see Fig. 2). Each scheme was implemented in Simulink/SPS and in real-time LabVIEW on the NI-PXI 8108. To guarantee the same conditions for comparison, the tests are started with the same initial conditions (battery SOC $= 70\%$, battery temperature $= 30$ °C, supercapacitor voltage $= 270$ V, supercapacitor temperature $= 25$ °C, fuel-cell voltage $= 52$ V, fuel-cell temperature $= 40$ °C). In addition, each scheme was implemented following the energy management requirement (see Table I).

The SOC reference for the classical PI control scheme is set to $\mathrm{SOC}_{\min}$ (60%) to have a fair comparison with other schemes. The load profile used for performance comparison is obtained by repeating the scenario depicted in Fig. 1 for 30 min, as shown in Fig. 21.

A. Power Distribution, Battery SOC, and Supercapacitor Voltage

The fuel-cell power (in watts) and battery power (in watts) at the 270-V dc bus (i.e., considering the converter losses) are shown in Fig. 22 for each scheme. The battery SOC (in percentage) and supercapacitor voltage (in volts) are also shown. The experimental results are shown on the right [see Fig. 22(b), (d), (f), (h), (j)], and the simulation results on the left [Fig. 22(a), (c), (e), (g), (h)].

As observed, the performances obtained from experiments correspond with the simulation. For the state machine control scheme [see Fig. 22(a) and (b)], the fuel cell follows the load until the battery SOC reaches its minimum; then, it tries to recharge the battery afterward. When the battery SOC reaches it minimum, the supercapacitors are charged more often by the fuel cell above their reference voltage (270 V), which forces

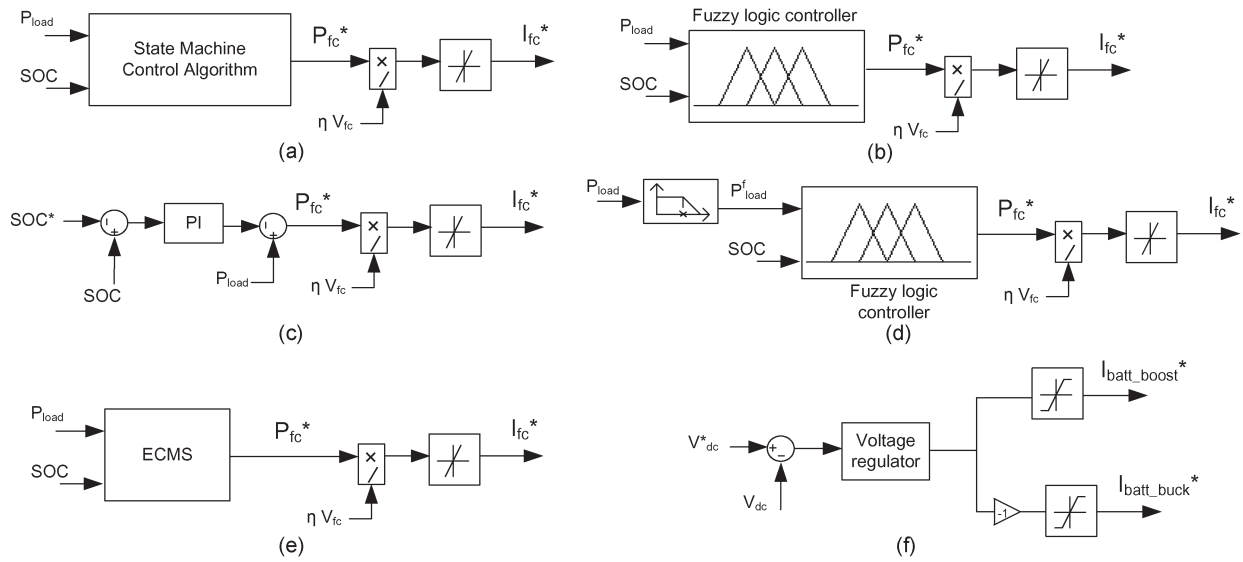

Fig. 18. Energy management schemes. (a) State machine control. (b) Rule-based fuzzy logic. (c) classical PI control. (d) frequency decoupling and fuzzy logic. (e) ECMS. (f) DC-bus voltage control common to all EMSs.

TABLE II
STATE MACHINE CONTROL DECISIONS

STATE MACHINE CONTROL DECISIONS			
If SOC High	& $P_{load} < Pfc_{min}$	state=1	$Pfc^* = Pfc_{min}$
If SOC High	& $P_{load} \in [Pfc_{min}, Pfc_{max}]$	state=2	$Pfc^* = P_{load}$
If SOC High	& $P_{load} \geq Pfc_{max}$	state=3	$Pfc^* = Pfc_{max}$
If SOC Normal	& $P_{load} < Pfc_{opt}$	state=4	$Pfc^* = Pfc_{opt}$
If SOC Normal	& $P_{load} \in [Pfc_{opt}, Pfc_{max}]$	state=5	$Pfc^* = P_{load}$
If SOC Normal	& $P_{load} \geq Pfc_{max}$	state=6	$Pfc^* = Pfc_{max}$
If SOC Low	& $P_{load} < Pfc_{max}$	state=7	$Pfc^* = P_{load} + P_{char}$
If SOC Low	& $P_{load} \geq Pfc_{max}$	state=8	$Pfc^* = Pfc_{max}$

SOC High → $SOC > SOC_{max}$ $\quad Pchar = -Pbatt_{min}$
SOC Normal → $SOC \in [85, 65]$
SOC Low → $SOC < SOC_{min}$

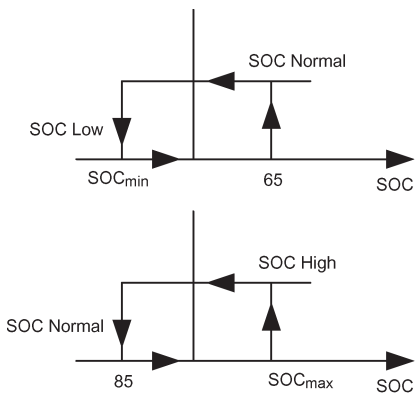

Fig. 19. State machine control hysteresis.

the dc-bus voltage regulator to request a negative current to recharge the battery.

In the rule-based fuzzy logic scheme [see Fig. 22(c) and (d)], as expected, the fuel-cell response is faster and smooth as the battery SOC becomes close to its minimum. When the battery SOC reaches its minimum, the fuel cell behaves as in the state machine control.

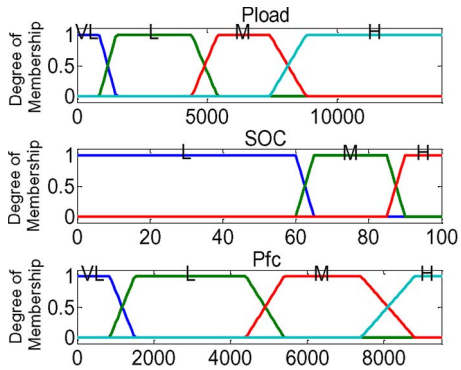

Fig. 20. Membership functions.

TABLE III
FUZZY LOGIC RULES

FUZZY LOGIC RULES			
If SOC H	&	P_{load} VL	Pfc* = VL
If SOC H	&	P_{load} L	Pfc* = L
If SOC H	&	P_{load} M	Pfc* = M
If SOC H	&	P_{load} H	Pfc* = H
If SOC M	&	P_{load} VL	Pfc* = VL
If SOC M	&	P_{load} L	Pfc* = L
If SOC M	&	P_{load} M	Pfc* = M
If SOC M	&	P_{load} H	Pfc* = H
If SOC L	&	P_{load} VL	Pfc* = L
If SOC L	&	P_{load} L	Pfc* = M
If SOC L	&	P_{load} M	Pfc* = H
If SOC L	&	P_{load} H	Pfc* = H

H → High M → Medium L → Low VL → Very Low

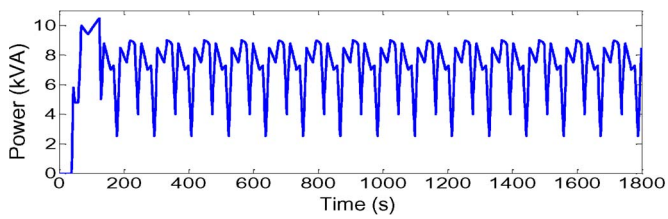

Fig. 21. Load profile of a 30-min emergency landing scenario.

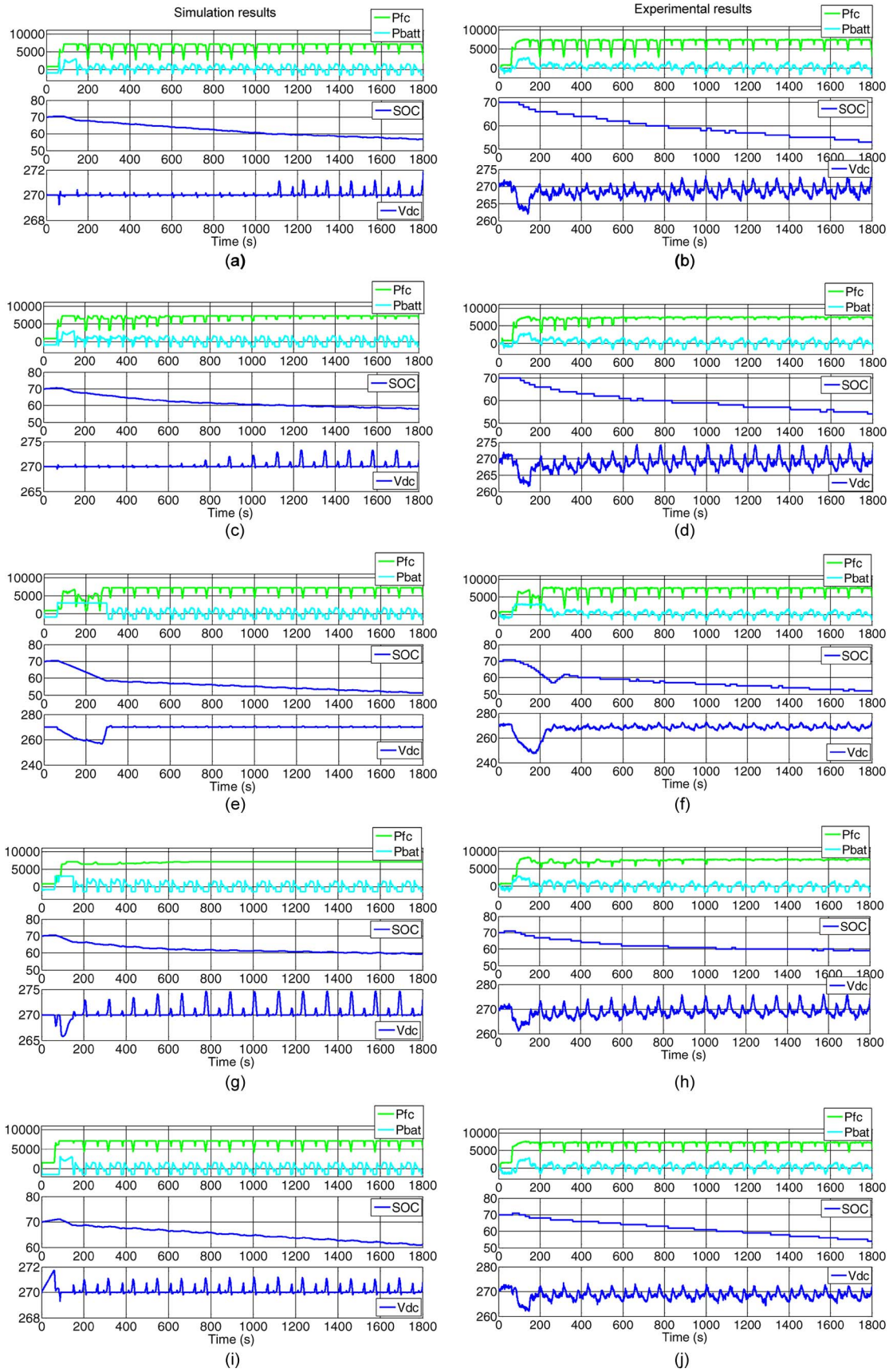

Fig. 22. Simulation and experimental results for all EMS schemes. (a) Simulation results for state machine control. (b) Experimental results for state machine control. (c) Simulation results for rule-based fuzzy logic. (d) Experimental results for rule-based fuzzy logic. (e) Simulation results for classical PI control. (f) Experimental results for classical PI control. (g) Simulation results for frequency decoupling and fuzzy logic. (h) Experimental results for frequency decoupling and fuzzy logic. (i) Simulation results for ECMS. (j) Experimental results for ECMS.

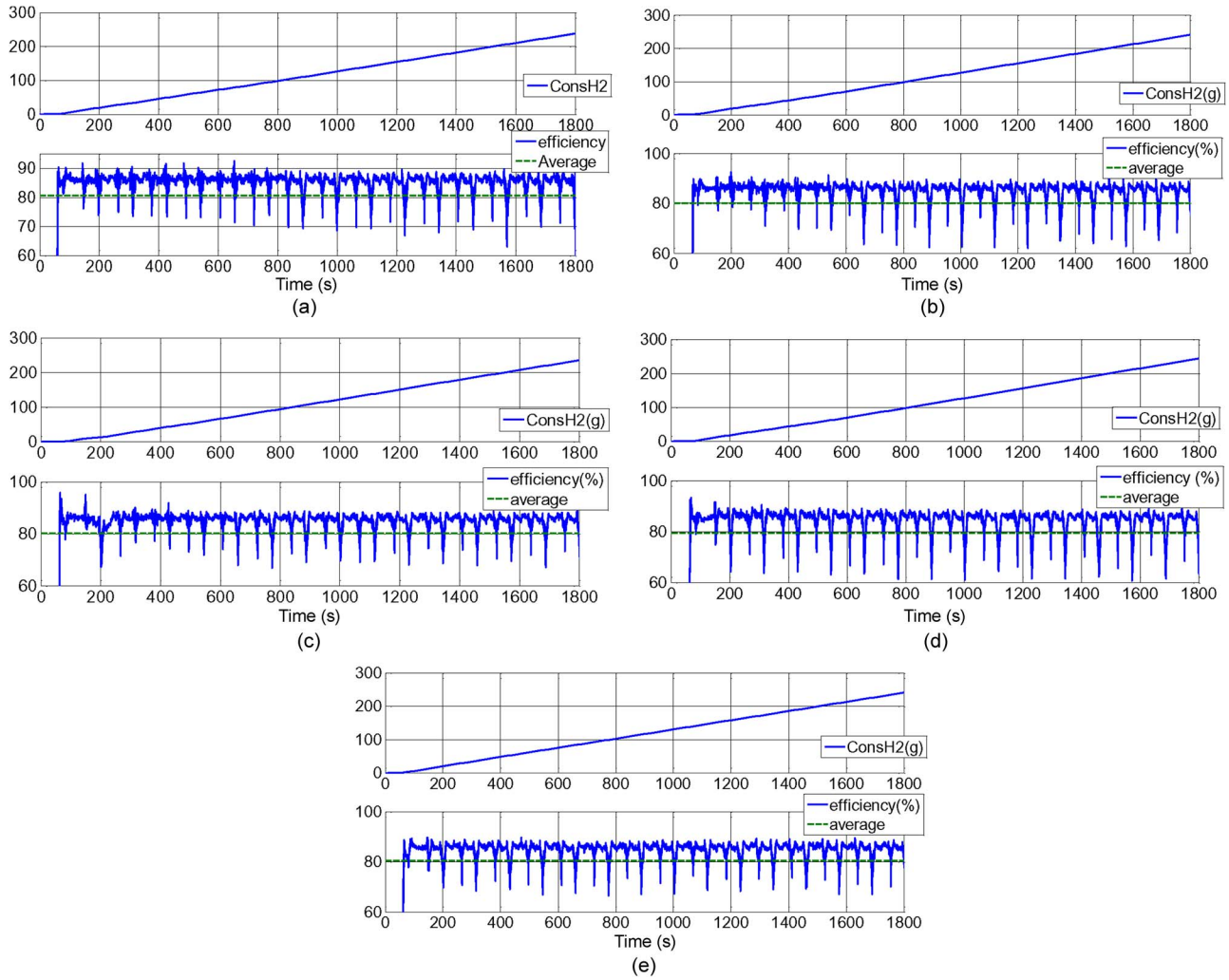

Fig. 23. Experimental results for all EMS schemes on hydrogen consumption and overall efficiency. (a) State machine control. (b) Rule-based fuzzy logic. (c) Classical PI control. (d) Frequency decoupling and fuzzy logic. (e) ECMS.

In the case of the classical PI control scheme [see Fig. 22(e) and (f)], the battery discharges faster to get to the SOC reference; afterward, the fuel cell tries to provide the load power and recharge the battery. Initially, the fuel-cell reference power is low, and the supercapacitors discharge to help the battery; consequently, the dc-bus voltage goes below the reference voltage. This can be avoided if the SOC reference is set to the initial battery SOC, but then, the comparison with other schemes will not be fair.

The frequency decoupling and fuzzy logic scheme [see Fig. 22(g) and (h)] forces the fuel cell to provide a nearly constant power, which allows the battery to recharge more often than the previous schemes. As observed, this scheme provides the lowest use of the battery energy (SOC between 70%–59%). A higher cutoff frequency (close to the air compressor response) can be used, which will make this scheme behaves as others, but the main objective of this scheme (which is to reduce the stress on the fuel-cell system and achieve a nearly zero battery energy) will not be satisfied.

A better performance is obtained for the ECMS scheme in simulation compared with experiments [see Fig. 22(i) and (j)]. The experimental results show more battery energy used. This is due to the noise sensibility of the optimization algorithm to measurements. However, the power distribution corresponds to simulations.

B. Hydrogen Consumption and Overall Efficiency

The hydrogen consumption and overall efficiency obtained from all schemes are calculated as follows.

The hydrogen consumption (in grams) is given by

$$\text{ConsH2} = \frac{N}{F}\int_0^{1800} i_{\text{fc}}dt \tag{16}$$

where F is the Faraday constant (in A · s/mol).

The overall efficiency is given by

$$\text{efficiency} = \frac{P_{\text{load}}}{P_{\text{fc}}^{\text{in}} + P_{\text{batt}}^{\text{in}} + P_{\text{cap}}^{\text{in}}} \tag{17}$$

where $P_{\text{fc}}^{\text{in}}$, $P_{\text{batt}}^{\text{in}}$, and $P_{\text{cap}}^{\text{in}}$ are the fuel-cell power (input to the dc/dc converter), battery power (input to the dc/dc converters), and supercapacitor power, respectively.

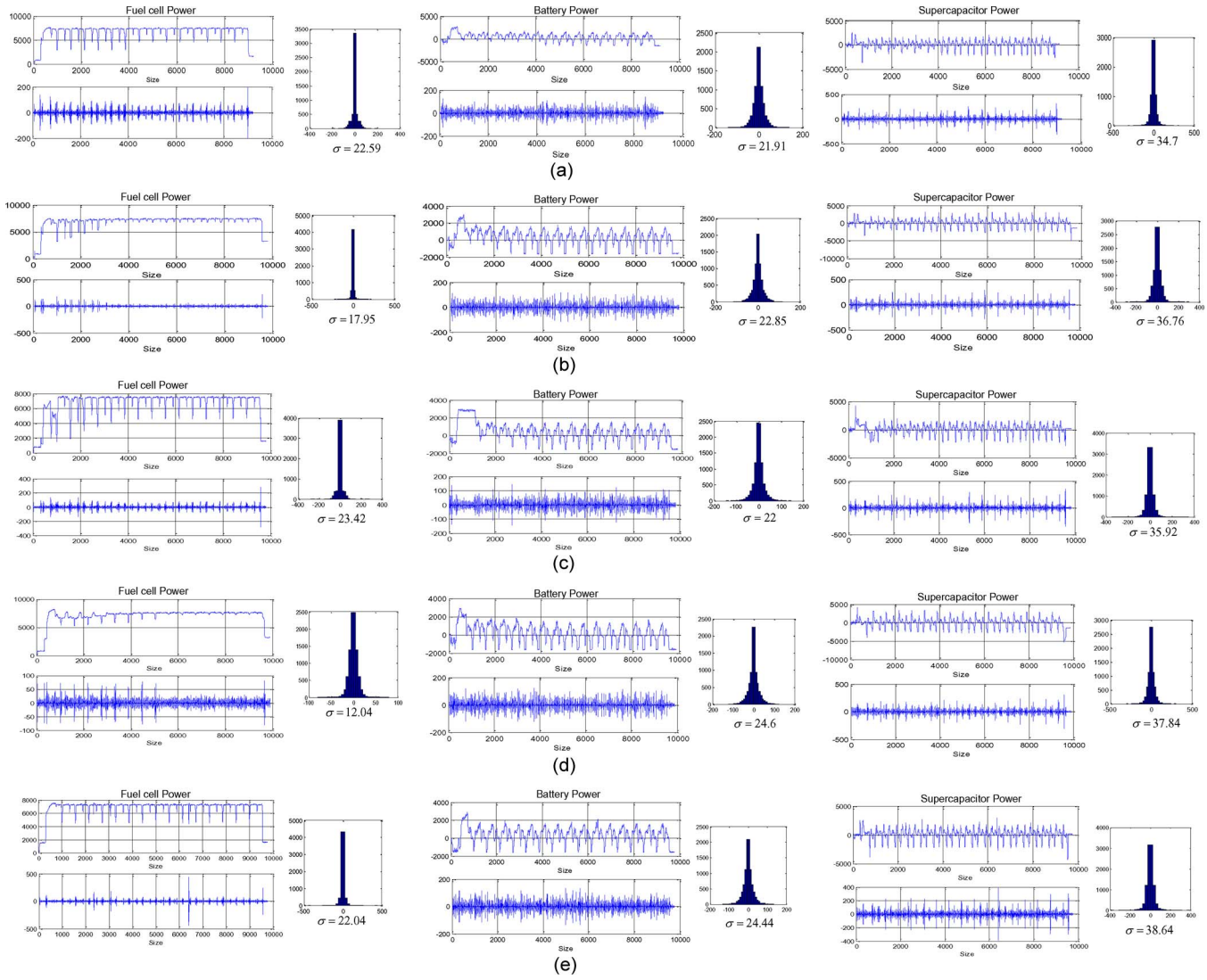

Fig. 24. Experimental results for all EMS schemes on stress analysis. (a) State machine control. (b) Rule-based fuzzy logic. (c) Classical PI control. (d) Frequency decoupling and fuzzy logic. (e) ECMS.

Fig. 23 shows the hydrogen consumption and efficiency obtained for all schemes from experiments. It can be noted that the state machine control [see Fig. 23(a)] is slightly more efficient than the other schemes, whereas the classical PI regulator has the lowest fuel consumption [see Fig. 23(c)]. In addition, the frequency decoupling scheme has the lowest overall efficiency and the highest fuel consumption [see Fig. 23(d)]. A summary (in tabular form) showing the results obtained for each scheme is provided in the following.

C. Stress Analysis

The stress on each energy source is determined with a new approach based on the wavelet transform of the fuel-cell power, battery power, and supercapacitor power at the 270-V dc bus. Each power is decomposed in low- and high-frequency components using the Haar wavelet decomposition, available in the MATLAB wavelet toolbox. The high-frequency component of each power has a mean value of zero, and the histogram or standard deviation σ of this component gives a good indication of how often each energy source is solicited.

Fig. 24 shows the experimental results obtained for each scheme. It is observed that the state machine control scheme has the lowest battery and supercapacitor stresses [see Fig. 24(a)], whereas the frequency decoupling and fuzzy logic scheme provides the lowest stress on the fuel-cell system.

The overall performance of all schemes based on the comparison criteria is summarized in Table IV.

VI. Conclusion

This paper has presented a performance comparison of different energy management schemes for a fuel-cell hybrid emergency system of MEA. The hybrid system is modeled and validated with experiments. Five state-of-the-art commonly used energy management schemes are studied through simulations and experimental tests on a 14-kW fuel-cell hybrid system. The same initial condition is used for all the schemes, and the experimental results are close to simulations. The

TABLE IV
OVERALL PERFORMANCE OF EACH EMS SCHEME

EMS / Criteria	State machine control	Rule based fuzzy logic	Classical PI control	Frequency decoupling & Fuzzy logic	ECMS
Battery SOC (%)	70 – 54	70 – 54	70 – 51	70 – 59	70 – 54
H2 Consumption (g)	238	240.6	235	245	240
Overall efficiency (%)	80.72	80.1	80.28	79.32	80.47
Fuel cell stress σ	22.59	17.95	23.42	12.04	22.04
Battery stress σ	21.91	22.85	22	24.6	24.44
Supercap. Stress σ	34.7	36.76	35.92	37.84	38.64

criteria for performance comparison are the hydrogen consumption, the battery SOC, the overall efficiency, and the stress seen by each energy source. The latter is measured using a new approach based on wavelet transform. Compared with the other schemes, the state machine control scheme provided slightly better efficiency (80.72%) and stresses on the battery and supercapacitor (σ of 21.91 and 34.7, respectively). The classical PI control scheme had the lowest fuel consumption (235 g of H_2 consumed) and more use of the battery energy (SOC between 70%–51%). As expected, the lowest fuel-cell stress (σ of 12.04) and the lowest use of the battery energy (SOC between 70%–59%) were achieved with the frequency decoupling and fuzzy logic scheme but at the expense of more fuel consumption (245 g of H_2 consumed) and lower overall efficiency (79.32%). The dc-bus or supercapacitor voltage was maintained nearly constant ($\approx$270 V_{dc}) for all the schemes. To conclude, the energy management system suitable for MEA should be a multischeme EMS, such that each scheme is chosen based on a specific criterion to prioritize. As an example, depending on the operating life of each energy source, the EMS can be chosen to either minimize the stress on the fuel-cell system, the battery system, or the supercapacitor system, hence maximizing the life cycle of the hybrid power system. In addition, if the target is to reduce the fuel consumption, the strategy based on the classical PI or ECMS could be selected. An alternative is to design a multiobjective optimization EMS to optimize all the performance criteria, which is the next topic for further studies.

REFERENCES

[1] P. Thounthong and S. Rael, "The benefits of hybridization," *IEEE Ind. Electron. Mag.*, vol. 3, no. 3, pp. 25–37, Sep. 2009.

[2] P. Thounthong, S. Rael, and B. Davat, "Control strategy of fuel cell and supercapacitors association for a distributed generation system," *IEEE Trans. Ind. Electron.*, vol. 54, no. 6, pp. 3225–3233, Dec. 2007.

[3] Z. Amjadi and S. Williamson, "Power-electronics-based solutions for plug-in hybrid electric vehicle energy storage and management systems," *IEEE Trans. Ind. Electron.*, vol. 57, no. 2, pp. 608–616, Feb. 2010.

[4] G. Renouard-Vallet, M. Saballus, G. Schmithals, J. Schirmer, J. Kallo, and A. K. Friedrich, "Improving the environmental impact of civil aircraft by fuel cell technology: Concepts and technological progress," *Energy Environ. Sci.*, vol. 3, no. 10, pp. 1458–1468, 2010.

[5] G. Renouard-Vallet, M. Saballus, G. Schmithals, J. Schirmer, J. Kallo, and A. K. Friedrich, "Fuel cells for aircraft applications," *ECS Trans.*, vol. 30, no. 1, pp. 271–280, 2011.

[6] X. Roboam, B. Sareni, and A. D. Andrade, "More electricity in the air: Toward optimized electrical networks embedded in more-electrical aircraft," *IEEE Ind. Electron. Mag.*, vol. 6, no. 4, pp. 6–17, Dec. 2012.

[7] W. Jiang and B. Fahimi, "Active current sharing and source management in fuel cell-battery hybrid power system," *IEEE Trans. Ind. Electron.*, vol. 57, no. 2, pp. 752–761, Feb. 2010.

[8] P. Garcia, L. M. Fernandez, C. A. Garcia, and F. Jurado, "Energy management system of fuel-cell-battery hybrid tramway," *IEEE Trans. Ind. Electron.*, vol. 57, no. 12, pp. 4013–4023, Dec. 2010.

[9] J. Ke, R. Xinbo, Y. Mengxiong, and X. Min, "A hybrid fuel cell power system," *IEEE Trans. Ind. Electron.*, vol. 56, no. 4, pp. 1212–1222, Apr. 2009.

[10] S. Caux, W. Hankache, M. Fadel, and D. Hissel, "On-line fuzzy energy management for hybrid fuel cell systems," *Int. J. Hydrogen Energy*, vol. 35, no. 5, pp. 2134–2143, Mar. 2010.

[11] L. Chun-Yan and L. Guo-Ping, "Optimal fuzzy power control and management of fuel cell/battery hybrid vehicles," *J. Power Sources*, vol. 192, no. 2, pp. 525–533, Jul. 15, 2009.

[12] X. Zhang, M. C. Chunting, A. Masrur, and D. Daniszewski, "Wavelet-transform-based power management of hybrid vehicles with multiple on-board energy sources including fuel cell, battery and ultracapacitor," *J. Power Sources*, vol. 185, no. 2, pp. 1533–1543, Dec. 1, 2008.

[13] B. Vural, A. R. Boynuegri, I. Nakir, O. Erdinc, A. Balikci, M. Uzunoglu, H. Gorgun, and S. Dusmez, "Fuel cell and ultra-capacitor hybridization: A prototype test bench based analysis of different energy management strategies for vehicular applications," *Int. J. Hydrogen Energy*, vol. 35, no. 20, pp. 11 161–11 171, Oct. 2010.

[14] P. Rodatz, G. Paganelli, A. Sciarretta, and L. Guzzella, "Optimal power management of an experimental fuel cell/supercapacitor-powered hybrid vehicle," *Control Eng. Pract.*, vol. 13, no. 1, pp. 41–53, Jan. 2005.

[15] L. Xu, J. Hua, J. Li, and M. Ouyang, "Distributed control system based on CAN bus for fuel cell/battery hybrid vehicle," in *Proc. IEEE ISIE*, Jul. 5–8, 2009, pp. 183–188.

[16] P. Garcia, J. P. Torreglosa, L. M. Fernandez, and F. Jurado, "Viability study of a FC-battery-SC tramway controlled by equivalent consumption minimization strategy," *Int. J. Hydrogen Energy*, vol. 37, no. 11, pp. 9368–9382, Jun. 2012.

[17] F. Savoye, P. Venet, M. Millet, and J. Groot, "Impact of periodic current pulses on li-ion battery performance," *IEEE Trans. Ind. Electron.*, vol. 59, no. 9, pp. 3481–3488, Sep. 2012.

[18] W. Greenwell and A. Vahidi, "Predictive control of voltage and current in a fuel cell-ultracapacitor hybrid," *IEEE Trans. Ind. Electron.*, vol. 57, no. 6, pp. 1954–1963, Jun. 2010.

[19] K. Min-Joong and P. Huei, "Power management and design optimization of fuel cell/battery hybrid vehicles," *J. Power Sources*, vol. 165, no. 2, pp. 819–832, Mar. 20, 2007.

[20] J. Moreno, M. E. Ortuzar, and J. W. Dixon, "Energy-management system for a hybrid electric vehicle, using ultracapacitors and neural networks," *IEEE Trans. Ind. Electron.*, vol. 53, no. 2, pp. 614–623, Apr. 2006.

[21] W. S. Lin and C. H Zheng, "Energy management of a fuel cell/ultracapacitor hybrid power system using an adaptive optimal-control method," *J. Power Sources*, vol. 196, no. 6, pp. 3280–3289, Mar. 15, 2011.

[22] P. Pisu and G. Rizzoni, "A comparative study of supervisory control strategies for hybrid electric vehicles," *IEEE Trans. Control Syst. Technol.*, vol. 15, no. 3, pp. 506–518, May 2007.

[23] A. Fadel and B. Zhou, "An experimental and analytical comparison study of power management methodologies of fuel cell-battery hybrid vehicles," *J. Power Sources*, vol. 196, no. 6, pp. 3271–3279, Mar. 15, 2011.

[24] J. Padulles, G. W. Ault, and J. R. McDonald, "An integrated SOFC plant dynamic model for power systems simulation," *J. Power Sources*, vol. 86, no. 1/2, pp. 495–500, Mar. 2000.

[25] S. M. Njoya, O. Tremblay, and L.-A. Dessaint, "A generic fuel cell model for the simulation of fuel cell vehicles," in *Proc. IEEE VPPC*, Sep. 7–10, 2009, pp. 1722–1729.

[26] O. Tremblay, L.-A. Dessaint, and A.-I. Dekkiche, "A generic battery model for the dynamic simulation of hybrid electric vehicles," in *Proc. IEEE VPPC*, Sep. 9–12, 2007, pp. 284–289.
[27] V. Musolino, L. Piegari, and E. Tironi, "New full-frequency-range supercapacitor model with easy identification procedure," *IEEE Trans. Ind. Electron.*, vol. 60, no. 1, pp. 112–120, Jan 2013.
[28] K. B. Oldham, "A Gouy–Chapman–Stern model of the double layer at a (metal)/(ionic liquid) interface," *J. Electroanal. Chem.*, vol. 613, no. 2, pp. 131–138, Feb. 2008.

Souleman Njoya Motapon (M'09) received the Higher Diploma from the Islamic University of Technology, Dhaka, Bangladesh, in 2002, the M.Sc. degree from Aalborg University, Aalborg, Denmark, in 2005; the M.Ing. and Ph.D. degrees from the Ecole de Technologie Superieure, Montreal, QC, Canada, in 2008 and 2013, respectively, all in electrical engineering.

He is currently a Researcher in the fields of power electronics at the Ecole de Technologie Superieure. From 2011 to 2012, he was with Clipper Windpower/Pratt & Whitney Power Systems, as a Senior Electrical Engineer in charge of next-generation turbine power conversion system design and simulation.

Louis-A. Dessaint (M'88–SM'91–F'13) received the B.Ing., M.Sc.A., and Ph.D. degrees from the École Polytechnique de Montréal, Montreal, QC, Canada, in 1978, 1980, and 1985, respectively, all in electrical engineering.

He is currently a Professor, the Hydro-Quebec/TransEnergie Chair on Simulation and Control of Power Systems, and the Head of the Department of Electrical Engineering with the Ecole de Technologie Superieure (ETS), Montreal. He is the author of The MathWorks "SimPowerSystems" Block Set.

Dr. Dessaint is a Fellow of the Canadian Academy of Engineering and a member of the Circle of Excellence of the University of Quebec. He is also an Associate Editor for the IEEE TRANSACTIONS ON CONTROL SYSTEMS TECHNOLOGY.

Kamal Al-Haddad (S'82–M'88–SM'92–F'07) received the B.Sc.A. and M.Sc.A. degrees from the University of Quebec in Trois-Rivières, Trois-Rivières, QC, Canada, in 1982 and 1984, respectively, and the Ph.D. degree from the National Polytechnic Institute of Toulouse, Toulouse, France, in 1988.

From June 1987 to June 1990, he was a Professor with the Department of Engineering, University of Quebec in Trois-Rivières. Since June 1990, he has been a Professor with the Department of Electrical Engineering, Ecole de Technologie Superieure (ETS), Montreal, QC, where he has been the Canada Research Chair in Electric Energy Conversion and Power Electronics since 2002. He has supervised more than 80 Ph.D. and M.Sc.A. students working in the fields of power electronics. From 1992 to 2003, he was the Director of graduate study programs at the ETS. He is a Consultant and has established a very solid link with many Canadian industries working in the fields of power electronics, electric transportation, aeronautics, and telecommunications. He is the Chief of the ETS–Bombardier Transportation North America Division, which is a joint industrial research laboratory on electric traction system and power electronics. He is a coauthor of the Power System Block Set software of MATLAB. He is the author or coauthor of more than 300 journal and conference papers. His research interests include high-efficiency static power converters, harmonics, and reactive power control using hybrid filters, switch mode, and resonant converters, including the modeling, control, and development of prototypes for various industrial applications in electric traction, power supply for drives, telecommunications, etc.

Prof. Al-Haddad is a Fellow of the Canadian Academy of Engineering and a Life Member of the Circle of Excellence of the University of Quebec. He is active in the IEEE Industrial Electronics Society, where he is Vice President for Technical Activities, an Administrative Committee Member, and a Distinguished Lecturer. He serves as an Associate Editor for the IEEE TRANSACTIONS ON INDUSTRIAL INFORMATICS. He was a recipient of the Outstanding Researcher Award from ETS in 2000.